μFLU08-154

A NAVIER-STOKES MODEL INCORPORATING THE EFFECTS OF NEAR-WALL MOLECULAR COLLISIONS WITH APPLICATIONS TO MICRO GAS FLOWS

Erik J. Arlemark[1], S. Kokou Dadzie & Jason M. Reese
Department of Mechanical Engineering
University of Strathclyde
Glasgow G1 1XJ
United Kingdom
erik.arlemark@strath.ac.uk, kokou.dadzie@strath.ac.uk,
jason.reese@strath.ac.uk

KEY WORDS

micro gas flows, Navier-Stokes equations, mean free path, non linear constitutive relationships, velocity slip

ABSTRACT

We propose a model for describing surface effects on micro gas flows. This model consists of the Navier-Stokes equations (NS) with discontinuous velocity slip boundary conditions and a description of a geometry-dependent and effective viscosity due to special consideration of the molecular collisions with solid boundaries. By extending NS with an effective viscosity we obtain a non-linear stress/strain-rate relationship which captures some of the near-wall effects that the conventional NS are unable to describe. We show results of NS extended by using our effective viscosity applied with Maxwell's boundary condition as well as a second order boundary condition achieved by partly incorporating higher order methods, the Maxwell-Burnett boundary condition proposed by Lockerby et al. (2004). With this proposed model the simple isothermal planar channel case of 2D Poiseuille flow is solved. The results of our proposed model are compared with the conventional NS using similar boundary conditions, the BGK-method and experiments. On the one hand it is seen that our extended NS model yields results that are asymptotic to the results of conventional NS for large flow scales. On the other hand, when comparing results on the micro scale, we see that our extended NS model yields results that are closer to the results of the BGK-method and the experiments than the conventional NS. Our extended NS-model shows signs of capturing the physics of the flow to a certain rarefaction degree where it does not predict the mass flow minimum shown by the BGK-method and the experiments.

[1] Corresponding author

1. INTRODUCTION

Interest in micro channel flows has grown with the recent vast improvements in manufacturing techniques on the microscale. Techniques for manufacturing micro turbines, fuel cells and MEMS (micro electronic mechanical systems) are today becoming reality, but as we reach production of yet smaller devices it is also realised that microscale gas flows cannot be modelled in the same way as macroscale flows. Further research into modelling microscale gas flows is therefore needed in order to understand and more effectively manufacture devices in which micro gas flows occur. [1]

To describe the degree of rarefaction, or state of non-equilibrium, of gas flows the key parameter is the Knudsen number,

$$Kn = \frac{\lambda}{L}. \tag{1}$$

This parameter expresses the ratio of the average travelling distance of molecules between collisions i.e. the mean free path, λ, to the characteristic length scale of the flow, L. We consider flow configurations comprising planar wall channels in this study, and will therefore use the channel height, H, as a measure of the length scale.

In micro gas flows, recognised by large Kn due to small length-scales, certain rarefaction effects become apparent. Experiments, such as those performed by Arkilic [2] and Colin [3] have shown that Navier-Stokes equations (NS) at relatively large Kn cannot capture the right mass flow rates without having a slip boundary condition applied. The argument for using the conventional non-discontinuous boundary conditions, commonly applied to NS, is valid for cases where the gas is in a state of near-equilibrium. Since micro gas flows of relatively large Kn depart from near-equilibrium these gas flows do not necessarily follow the no-slip boundary conditions. The lower threshold value for applying a slip boundary condition is generally at $Kn = 0.01$, which therefore commonly is referred to as the lower limit of the slip regime. For gas flows at even larger Kn further modelling modifications are needed because the linear constitutive relationship of NS breaks down, which happens at about Kn 0.1. This level is the lower limit of the transition regime which is characterised by being in between a continuum description and a free molecular description and is the regime that we mostly focus on for modelling improvements. Due to the simplicity of NS it is often desirable to solve flow cases with this solution method for as high Kn flows as possible. A proposed method of extending the validity of NS to large Kn was proposed by Erik Arlemark *et al.* [4], where molecular interactions with the wall were incorporated. Here we use the same method applied with the first order boundary condition as well as a second order boundary condition and concentrate on Poiseuille flow predictions and mass flow rate.

2. VELOCITY SLIP

An early velocity slip boundary condition is proposed by Maxwell [4], and has the following form for isothermal cases:

$$\boldsymbol{U}_{\text{slip}} = \pm\frac{2-\sigma}{\sigma}\frac{\lambda}{\mu}\tau_{\text{wall}}, \tag{2}$$

where $\boldsymbol{U}$ is the mass average velocity, τ is the stress tensor and μ is the dynamic viscosity. The tangential momentum accommodation coefficient, σ, describes the proportion of molecules being reflected diffusively ($\sigma = 1$) from the wall as opposed to those that experience specular reflections ($\sigma = 0$). If the reflections of the molecules are diffusive their tangential momentum is, on average, lost relative to the wall as opposed to specular reflections where the tangential momentum is kept. Here we will only consider purely diffusive reflections. In (2) "slip" denotes the discontinuous velocity difference between the wall and the gas next to the wall. The notation "wall" is used to describe a quantity that is taken at the boundary. The "±" sign is determined dependent on whether the wall normal coordinate increases or decreases with wall distance.

2.1 First Order Slip Model

We obtain a first order velocity slip by inserting the stress tensor of the NS equations into (2). The velocity slip for isothermal planar walls can then be expressed as:

$$\boldsymbol{U}_{\text{slip}} = -\frac{2-\sigma}{\sigma}\lambda\left(\frac{\partial \boldsymbol{U}}{\partial y}\right)_{\text{wall}}, \tag{3}$$

where y is the coordinate perpendicular to the wall which is zero in the middle of the channel.

2.2 Second Order Slip Model

Some investigators of micro gas flows mention that a second order slip boundary condition should be applied for gas flows in the transition regime [1,6,7]. There are several suggested formulations for second order boundary conditions, for planar walls most of which have the following form:

$$\boldsymbol{U}_{\text{slip}} = -A_1\lambda\left(\frac{\partial \boldsymbol{U}}{\partial y}\right)_{\text{wall}} - A_2\frac{\lambda^2}{2}\left(\frac{\partial^2 \boldsymbol{U}}{\partial y^2}\right)_{\text{wall}}, \tag{4}$$

where A_1 and A_2 are two modelling parameters. There are various proposals for what values these parameters should be set to. Some of the proposals are purely theoretically derived, whereas others have been obtained through comparisons with experimental results [6]. As listed by Karniadakis *et al.* [7], the coefficient A_1 is set to 1 by investigators like Deissler, Schamberg, Hsia and Domoto and Maxwell as opposed to Cercignani's A_1 value of 1.1466. The commonly applied value for the A_2 parameter varies in the wider range from -0.5 to $5\pi/12$.

A new high order boundary condition was proposed by Lockerby *et al.* [8] who used a high order stress tensor from the Burnett equations in (2). For isothermal planar wall configurations this high order slip boundary formulation is given by:

$$\boldsymbol{U}_{\text{slip}} = -\frac{2-\sigma}{\sigma}\lambda\left(\frac{\partial \boldsymbol{U}}{\partial y}\right)_{\text{wall}} - \frac{9}{4\pi}\frac{Pr(\gamma-1)}{\gamma}\frac{\lambda^2}{2}\left(\frac{\partial^2 \boldsymbol{U}}{\partial y^2}\right)_{\text{wall}}, \tag{5}$$

where Pr is the Prandtl number and γ is the specific heat ratio. This slip boundary condition varies with Pr and γ and therefore depends on what gas is studied. By comparing (4) and (5) we can identify the two modelling parameters A_1 and A_2 as follows:

$$A_1 = \frac{2-\sigma}{\sigma} \quad \text{and} \quad A_2 = \frac{9}{4\pi}\frac{Pr(\gamma-1)}{\gamma}. \tag{6}$$

In the next section we will propose a method for extending NS for micro gas flows by incorporating a non-linear stress/strain-rate relationship.

3 NAVIER-STOKES EQUATIONS AND GEOMETRY DEPENDENT VISCOSITY

Since micro gas flows are characterised by having a large ratio of confining boundary areas to their volumes, we study the flow behaviour when molecular collisions with the solid boundaries are involved in the description of viscosity. This modelling modification is expected to have a significant effect as opposed its negligible effect only for confined micro gases, not for larger scales of gas flows.

The commonly used relationship between the dynamic viscosity, μ, and the mean free path, λ, which is discussed in further depth by Cercignani [9] is expressed as follows:

$$\mu = \rho\frac{\lambda}{\sqrt{\pi/2RT}}, \tag{7}$$

where ρ is the gas density, R is the specific gas constant and T is the gas temperature. We propose that for micro gas flows the effect of the increasingly important molecular collisions with solid boundaries be incorporated in (7) by replacing the unconfined expression for a mean free path, λ, with an effective and geometry dependent mean free path, λ_{eff}. This yields a geometry-dependent effective viscosity, μ_{eff} which results in the new constitutive non-linear stress/strain-rate relationship for NS as follows:

$$\tau = -\mu_{\text{eff}}\left[\nabla \boldsymbol{U} + (\nabla \boldsymbol{U})^t\right] + \left(\frac{2}{3}\mu_{\text{eff}} - \kappa\right)(\nabla \cdot \boldsymbol{U})I, \tag{8}$$

where κ is the bulk viscosity, I is the identity tensor and t is the transpose operator. With (8) incorporated in NS, without external forces, this yields the new governing momentum equation:

$$\rho\frac{DU}{Dt} = -\nabla p + \nabla\cdot\left[\mu_{\text{eff}}\left[\nabla U + (\nabla U)^t\right] - \left(\frac{2}{3}\mu_{\text{eff}} - \kappa\right)(\nabla\cdot U)I\right], \tag{9}$$

where $D/Dt = \partial/\partial t + (U\cdot\nabla)$ is the material derivative. For many steady state micro gas flow situations the conventional NS equations can be reduced to the Stokes equation [7], which for our proposed method has the following form:

$$\nabla\cdot\mu_{\text{eff}}\left[\nabla U + (\nabla U)^t\right] = \nabla p. \tag{10}$$

In the next section we present our proposed λ_{eff}-expression and thereby μ_{eff}.

4. AN EFFECTIVE MEAN FREE PATH

The proposed effective mean free path, λ_{eff}, which describes a molecular mean free path affected by collisions with unyielding walls is derived in Arlemark *et al.* [4] for cases where the gas is confined by two infinitely wide walls that are planar and parallel to each other. We consider that the molecules of the gas are equally likely to travel in any azimuthal angle, θ, shown in figure 1. The dagger notations, †, in this model will be used to denote quantities for molecules that travel in a positive *y*-direction.

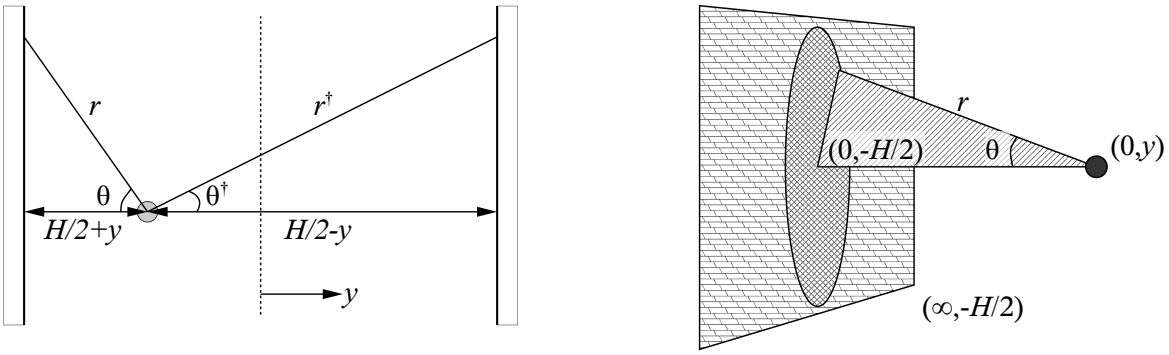

Figure 1: Left, a molecule confined between two planar walls separated by a wall distance *H, a* possible travelling path is denoted by *r*. Right, a three dimensional representation of a molecule close to a wall in a cylindrical coordinate system, where $r=(H/2+y)/\cos(\theta)$.

We use the probability function:

$$P = 1 - \exp\left(-\frac{r}{\lambda}\right), \tag{11}$$

to express the probability of a molecule travelling a distance *r* without experiencing a collision. The free path, *l*, is then obtained by weighting the unconfined mean free path, λ, with one half of the probability function *P*(r), which corresponds to the collision probability in cases where the molecule is moving in the negative *y*-direction, plus one half of $P(r^\dagger)$, which corresponds to the collision probability in cases where the molecule is moving in the positive y-direction. The free path is, by this reasoning, expressed as:

$$l = \lambda\times\frac{1}{2}\left[P(r) + P(r^\dagger)\right]. \tag{12}$$

The λ_{eff}-expression is then obtained by taking the integral mean value over all possible molecular travelling directions of θ and $\theta^\dagger$ in the range of $[-\pi/2, \pi/2]$ as follows:

$$\begin{aligned}\lambda_{\text{eff}} = &\frac{2}{\pi}\int_0^{\pi/2}\lambda\times\frac{1}{2}\left[1-\left[\exp\left(-\frac{H/2+y}{\lambda\cos\theta}\right)\right]\right]d\theta \\ &+\frac{2}{\pi}\int_0^{\pi/2}\lambda\times\frac{1}{2}\left[1-\left[\exp\left(-\frac{H/2-y}{\lambda\cos\theta^\dagger}\right)\right]\right]d\theta^\dagger,\end{aligned} \tag{13}$$

which allows us to express λ_{eff} in the form $\lambda_{\text{eff}} = \lambda\times K(y,\lambda,H)$. In this paper the integration to obtain K is

done by Simpson's numerical integration method using 8 equally sized intervals[2], which yields:

$$K(y,\lambda,H) = 1 - \frac{1}{46}\left[\exp\left(-\frac{H/2+y}{\lambda}\right) + \exp\left(-\frac{H/2-y}{\lambda}\right) + 4\left(\sum_{i=1}^{4}\exp\left(-\frac{H/2+y}{\lambda\cos(1/16\,(2i-1)\pi)}\right) + \exp\left(-\frac{H/2-y}{\lambda\cos(1/16\,(2i-1)\pi)}\right)\right) + 2\left(\sum_{i=1}^{3}\exp\left(-\frac{H/2+y}{\lambda\cos(1/8\,\pi i)}\right) + \exp\left(-\frac{H/2-y}{\lambda\cos(1/8\,\pi i)}\right)\right)\right]. \quad (14)$$

In the remainder of this paper we will focus on the y dependence of K, as the dependence on λ and H are determined through the rarefaction parameter Kn.

5. PLANAR POISEUILLE FLOW CASE

Here we calculate the velocity and the mass flow rate for isothermal fully developed Poiseuille flow in a planar wall channel using our proposed model. We use the modified Stokes equation, (10), and apply the first and second order boundary conditions in which λ is replaced by λ_{eff}. The solution method used here is the same as that in Kandlikar *et al.* [10], i.e. that the normalised velocity profile in a channel cross section of the flow is obtained by calculating the fully developed incompressible flow, but the density is recalculated using the ideal gas law in relation to temperature and pressure.

In our planar wall configuration, the Stokes equation is expressed in the following form:

$$\frac{\partial}{\partial y}\left[\mu_{\text{eff}}\frac{\partial U_x}{\partial y}\right] = \frac{\partial p}{\partial x}, \quad (15)$$

where the velocity of the flow in the axial direction (x-direction) of the channel is U_x, and this is assumed to vary only in the direction normal to the wall, the y-direction. We solve (15) using the first order boundary condition of (3) and then with the second order boundary condition of (5). From (6) the modelling parameter A_1 of the boundary conditions is here set to 1, since only diffusive reflections are considered. The parameter A_2 is set to 0.19, since the investigated gas is helium, which has a specific heat ratio, γ, of 5/3 and a Prandtl number of 2/3.

5.1 Velocity profile results

The expressions for the normalized velocity using the conventional NS, and our proposed extension to NS with an effective viscosity, NS_{eff}, are listed in table 1. These two models are solved using both first and second order boundary conditions, where λ is used for the conventional NS and λ_{eff} for the extended NS.

Model	**Normalised velocity profile**	
NS, first order BC:	$\frac{U_x}{U_0} = 1 - 4\left(\frac{y}{h}\right)^2 + 4A_1\frac{\lambda}{H}$	(16)
NS, second order BC:	$\frac{U_x}{U_0} = 1 - 4\left(\frac{y}{h}\right)^2 + 4A_1\frac{\lambda}{H} + 8A_2\frac{\lambda^2}{H^2}$	(17)
NS_{eff}, first order BC:	$\frac{U_x}{U_0} = \frac{8}{H^2}\left[G(H/2) + A_1\lambda\frac{H}{2} - G(y)\right]$	(18)
NS_{eff}, second order BC:	$\frac{U_x}{U_0} = \frac{8}{H^2}\left[G(H/2) + A_1\lambda\frac{H}{2} + A_2\lambda^2\left[K(H/2) - \frac{H}{2}K'(H/2)\right] - G(y)\right]$	(19)

Table 1: The four normalized solution equations for the gas flow velocity profiles using NS and our proposed NS with effective viscosity, NS_{eff}, for both first and second order boundary conditions, BC.

[2] The difference in mass flow results for 4 respectively 8 integration intervals is 2.2% for Kn = 8.86, which yields reason to believe that further increase of integration intervals will only marginally affect the results.

The following variables are used in table 1:

$$G(y) = \int \frac{y}{K(y)} dy, \quad U_0 = -\frac{H^2}{8\mu}\frac{dp}{dx} \quad \text{and} \quad K' = \frac{dK(y)}{dy}.$$

The results of the velocity profiles from the expressions in table 1 are shown in figure 2 and compared with the results of the BGK method provided by Sharipov [11]. We show results for three *Kn* cases: Kn_A = 0.113, Kn_B = 0.451 and Kn_C = 0.903, calculated using the unconfined λ-value. It is seen in figure 2 that for the Kn_A-case our proposed NS_{eff}-model using a second order boundary condition concides with the BGK model except near the wall where the latter is slightly lower. The velocity profile of NS_{eff} using the first order boundary condition is also reasonably close to the BGK model but slightly lower across the channel. The NS model using first and second order boundary conditions in the Kn_A-case are considerably lower than the BGK-model, except in the near wall area where they are on top of each other. For the Kn_B-case all the velocity profiles are separate from each other. It is however seen that the NS_{eff}-model using second order boundary condition is the closest to the BGK model, except in the near-wall area where none of the models correctly describe the velocity profile (although the models using first order boundary conditions have the same velocity slip). In the Kn_C-case all the velocity profiles are separated from each other, but our proposed NS_{eff} model using second order boundary conditions still presents the velocity profile which is most similar to the BGK-model. Although none of the models capture the right slip amount it is seen that the models using first order boundary conditions are closest to the BGK velocity profile at the wall.

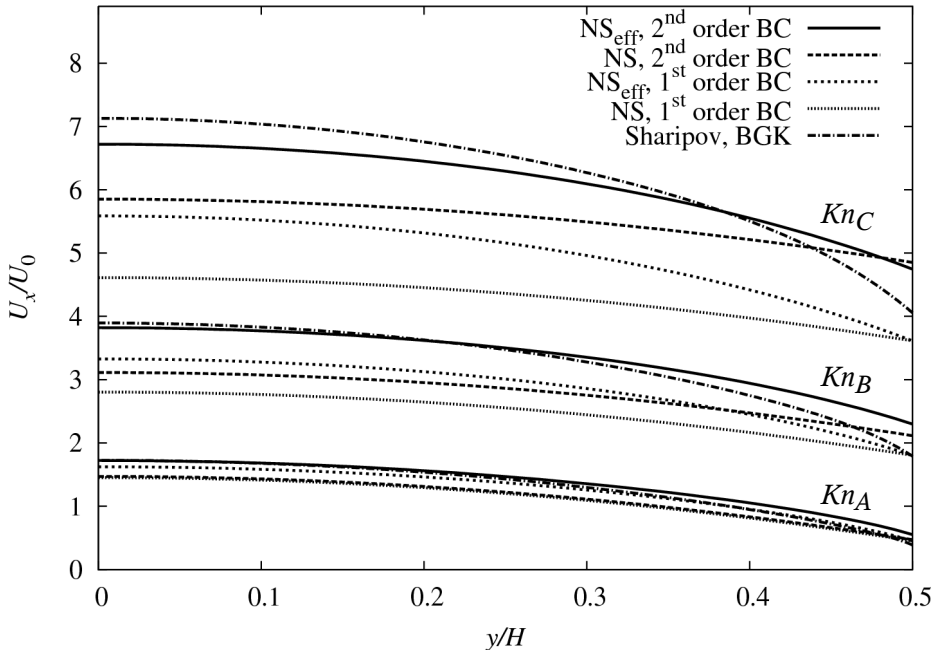

Figure 2: Half-channel Poiseuille flow velocity profiles from conventional NS and our proposed effective viscosity extended NS, NS_{eff}, using first and second order boundary conditions (BC) compared with BGK results of Sharipov [11]. The velocity profiles are for three different *Kn* i.e. Kn_A=0.113 (bottom), Kn_B=0.451 (middle) and Kn_C=0.903 (top). For Kn_A=0.113 the two NS velocity profiles are on top of each other.

5.2 Mass flow results

In this section we concentrate on the issue of comparing our results with experimental results by Ewart *et al.* [6] of mass flow rates for various rarefaction degrees. Ewart's experimental measurements are for helium gas, driven by a pressure difference ratio of 5 between the inlet and the outlet of the channel. Mass flow rates are obtained in the *Kn*-range of 0.03 to 50. The experimental channel dimensions that are used are: height, H=9.38μm; width, W=492μm; and length, L=9.39mm. Since this channel is reasonably wide compared to its height it is assumed that a comparison with our 2D model channel is valid.

In order to be able to compare our results with the experimental results the velocity dependent mass flux is calculated using the following relation:

$$\dot{m} = \rho \langle U_x \rangle A = \frac{p \langle U_x \rangle A}{RT}, \tag{20}$$

where A is the area of the cross section of the channel and

$$\widetilde{U}_x = \frac{\langle U_x \rangle}{U_0} = \frac{2}{H} \int_0^{H/2} \frac{U_x}{U_0} dy, \tag{21}$$

is the normalised average velocity across the channel width. We will here use the mass flow definition of (20) on the averaged velocities of the four NS-based velocity expressions (16)-(19) and normalise by the quantity

$$\dot{m}_0 = -\frac{AH}{\sqrt{2RT}} \frac{dp}{dx}. \tag{22}$$

We thereby obtain the normalised expression for the mass flux rate:

$$\frac{\dot{m}}{\dot{m}_0} = \frac{U_0}{m_0} \frac{pA}{RT} \widetilde{U}_x = \frac{\sqrt{\pi}}{8} \frac{H}{\lambda} \widetilde{U}_x. \tag{23}$$

Then (23) is expressed in terms of the inverse rarefaction parameter δ which is defined as follows:

$$\delta = \frac{H}{\lambda} \frac{\sqrt{\pi}}{2}. \tag{24}$$

The expression for the δ-dependent mass flow rate is then formulated as:

$$\frac{\dot{m}}{\dot{m}_0} = \frac{\delta}{4} \widetilde{U}_x(\delta). \tag{25}$$

The results for our model mass flow rates are shown in figure 3, together with the BGK results achieved by Sharipov [11] and the experimental results of Ewart *et al.* [6].

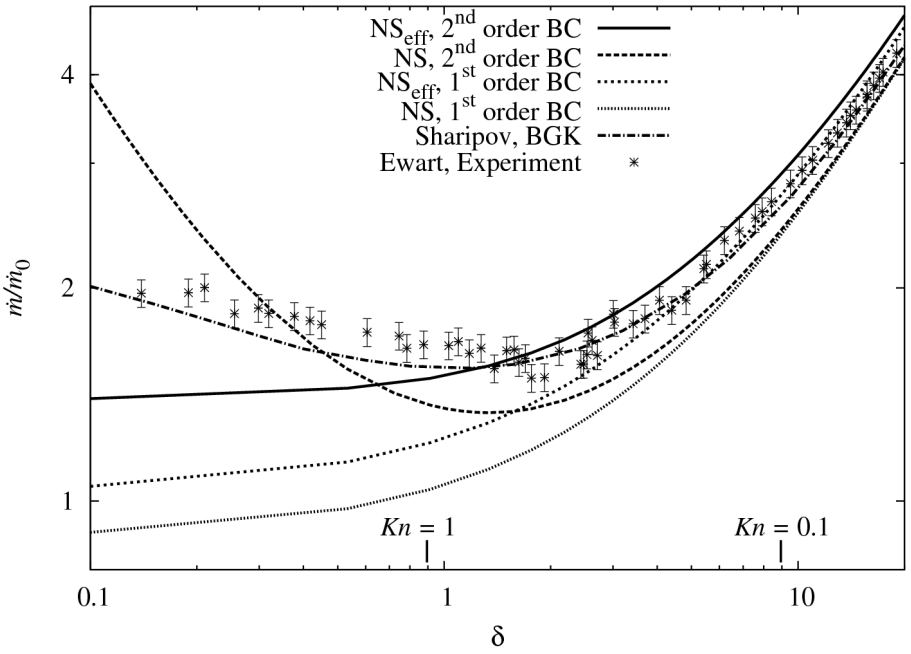

Figure 3: Mass flow results from NS and from our proposed NS-model using effective viscosity, NS_{eff}, using both first and second order boundary conditions (BC). The results are compared with BGK solutions by Sharipov [11] and experimental results by Ewart *et al.* [6]. The height of the error bars of the experimental data is set to 4.5% of the normalised mass flow rate values, consistent with Ewart's own data.

Although a simple model is prefered that describes flow characteristics correctly for the whole range of δ-values, it is found that the NS-based models are limited in effectiveness beyond a certain δ level. In table 2

the approximate range of applicability, within the δ-inspection range of 0.1 – 20, is listed for the various models. Here the applicability ranges are estimated by their ability to reproduce similar mass flow rates as the experimental data within a reasonable range of the error bars.

	Approximate range of applicability	
Model	In terms of δ	In terms of *Kn*
NS, first order BC:	15-20	0.04-0.06
NS, second order BC:	15-20	0.04-0.06
NS_{eff}, first order BC:	4-20	0.04-0.22
NS_{eff}, second order BC:	1-20	0.04-0.89
BGK	0.1-20	0.04-8.89

Table 2: List of the applicability ranges of the tested NS-based models, roughly estimated by visual comparison of model results with the experimental data of Ewart *et al.* [6] shown in figure 3.

It can be seen from figure 3 that all of the presented models, together with the experimental values, are asymptotic for low *Kn*, which strengthens our assumption that the influence of λ_{eff} and μ_{eff}, should have, a decaying effect with decreasing rarefaction degree. In figure 3 it is seen that our proposed NS_{eff}-model using the second order boundary condition has a slightly high mass flow rate at δ = 20, compared with the validation data of Sharipov [11] and Ewart *et al.* [6]. However, in figure 2 it is seen that the same model has a seemingly correct velocity profile for the lower *Kn* of 0.113. It is assumed that the high mass flow rate is due to the slightly higher velocity values in the near wall region. It should also be noted that for higher δ-values the mass flow results of the NS_{eff}-model using first order boundary conditions show better results compared to the NS_{eff}-model using second order boundary conditions. Among the NS-based models it is only the conventional NS model using the second order boundary condition that manages to produce a mass flow minimum at a δ value of about 1.5.

6. CONCLUSIONS AND DISCUSSIONS

A velocity slip boundary condition is commonly applied to the continuum Navier-Stokes equation (NS) for micro gas flows in the slip regime in order to achieve good results. In this paper we have provided a method which attempts to model micro gas flows in the low *Kn* region of the transition regime by incorporating a partly molecular description to the NS as well as in the conventional slip boundary condition. The molecular description consists of incorporating molecular collisions with boundaries into the conventional definition of the mean free path, which then becomes a geometry-dependent parameter. This new definition of the effective mean free path is then used to achieve an effective viscosity, which yields a non-linear stress/strain-rate relationship to the NS model.

By using the proposed extension to NS, and the first order boundary condition of Maxwell or the second order Maxwell-Burnett boundary conditions, we can extend the validity of NS to *Kn* = 0.22 and *Kn* = 0.89 respectively. It is found that the conventional NS using similar boundary conditions can satisfactory describe flows to a rarefaction degree of about *Kn* = 0.06. It should be noted that these conventional NS-models can produce results which fit our validation data better, for higher *Kn,* by choosing different values for the modelling parameters A_1 and A_2 of the boundary conditions. It is however decided to use $A_1 = 1$ which is consistent with the typical value used by different investigators [7] and the value of $A_2 = 0.19$ which is from an identification of gas properties. It is found that our proposed extended NS-model using first order boundary conditions makes a better gas flow description for lower *Kn* than the same model using the second order boundary conditions, which only coarsely captures the flow characteristics at higher *Kn* values.

It is seen in the mass flow results of figure 3 that only the conventional NS-model using the second order boundary condition managed to capture the mass flow minimum. Corrections to our λ_{eff}-description may be needed in order to capture the mass flow minimum within the framework of our continuum models. In the present work the λ_{eff}-description requires that intermolecular collisions should be accounted for in the

same way as molecular collisions with the boundaries. However intermolecular collision may cause a shortening of both molecules free paths, which is why we will investigate further the use of a modified formulation of the relation $\lambda_{\text{eff}} = \lambda \times K(y, \lambda, H)$ that takes these differences of collisions into account. We will also investigate the predictions of the molecular mean free paths in the presence of boundaries by molecular dynamics.

ACKNOWLEDGEMENTS

The authors would like to thank Simon Mizzi for helpful discussions and Timothée Ewart for providing experimental data. This research is funded in the UK by the Engineering and Physical Sciences Research Council under grant number EP/D007488/1.

REFERENCES AND CITATIONS

[1] Gad-el-Hak, M. (1999). Fluid mechanics of microdevices -the Freeman Scholar lecture. *Journal of Fluids Engineering, Transactions of the ASME*, **121** (1), 5–33.

[2] Arkilic, E., Schmidt, M., & Breuer, K. (1997). Gaseous slip flow in long microchannels. *Journal of Microelectromechanical Systems*, **6** (2), 167–178.

[3] Colin, S. (2005). Rarefaction and compressibility effects on steady and transient gas flows in microchannels. *Microfluidics and Nanofluidics,* **1,** 268-279.

[4] Arlemark, E. J., Dadzie, K. S. & Reese, J. M. (2008). An extension to the Navier-Stokes-Fourier equations by considering molecular collisions with boundaries. ASME ICNMM, Darmstadt, Germany. ICNMM2008-62222.

[5] Maxwell, J. C. (1879). On stresses in rarified gases arising from inequalities of temperature. *Philosophical Transactions of the Royal Society of London*, **170**, 231–256.

[6] Ewart, T., Perrier, P., Graur, I. A., & Meolans, J. G. (2007). Mass flow rate measurements in a microchannel, from hydrodynamic to near free molecular regimes. Journal of Fluid Mechanics, 584, 337 – 356.

[7] Karniadakis, G., Beskok, A., & Aluru, N. (2005). *Microflows and Nanoflows: Fundamentals and Simulation*. Springer.

[8] Lockerby, D. A., Reese, J. M., Emerson, D. R., & Barber, R. W. (2004). Velocity boundary condition at solid walls in rarefied gas calculations. *Physical Review E*, **70**, 017303.

[9] Cercignani, C. (2000). *Rarefied Gas Dynamics*, Cambridge University Press.

[10] Kandlikar, S., Garimella, S., Li, D., Colin, S., & King, M. R. (2005). *Heat Transfer and Fluid Flow in Minichannels and Microchannels*. Elsevier.

[11] Sharipov, F. M. (1999). Rarefied gas flow through a long rectangular channel. *Journal of Vacuum Science & Technology A: Vacuum Surfaces and Films*, **17**(5), 3062-3066.